energies

MDPI

Article

Seismic Description of Deep Strike-Slip Fault Damage Zone by Steerable Pyramid Method in the Sichuan Basin, China

Qingsong Tang [1], Shuhang Tang [2,*], Bing Luo [3], Xin Luo [3], Liang Feng [3], Siyao Li [2] and Guanghui Wu [2,*]

[1] PetroChina Southwest Oil & Gasfield Company, Chengdu 610051, China
[2] School of Geoscience and Technology, Southwest Petroleum University, Chengdu 610500, China
[3] Chongqing Division, PetroChina Southwest Oil & Gasfield Company, Chongqing 400707, China
* Correspondence: stang@swpu.edu.cn (S.T.); wugh@swpu.edu.cn (G.W.)

Abstract: Large quantities of gas resources have been found in the Paleo-Mesozoic carbonate rocks in the Sichuan Basin. However, many wells cannot obtain high production in deep low porosity-permeability reservoirs. For this contribution, we provide a steerable pyramid method for identifying the fault damage zone in the Kaijiang–Liangping platform margin, which is infeasible by conventional seismic methods. The results show that steerable pyramid processing could enhance the seismic fault imaging and a series of NW-trending strike-slip faults are found along the trend of the carbonate platform margin. The steerable pyramid attribute presents distinct vertical and horizontal boundaries of the fault damage zone, and heterogeneous intensity of an un-through-going damage zone. The width of the fault damage zone is generally varied in the range of 100–500 m, and could be increased to more than 1000 m in the fault overlap zone, intersection area, and fault tips. Further, the fault damage zone plays a constructive role in the high gas production in the deep tight carbonate reservoir. The results suggest the steerable pyramid method is favorable for identifying the weak strike-slip faults and their damage zone. The width of the fault damage zone is closely related to fault displacement, and the much wider damage zone is generally influenced by the fault overlapping and interaction. The fractured reservoirs in the fault damage zone could be a new favorable exploitation domain in the Sichuan Basin.

Keywords: steerable pyramid processing; strike-slip fault; fault damage zone; fractured reservoir; carbonate exploitation; Sichuan Basin

Citation: Tang, Q.; Tang, S.; Luo, B.; Luo, X.; Feng, L.; Li, S.; Wu, G. Seismic Description of Deep Strike-Slip Fault Damage Zone by Steerable Pyramid Method in the Sichuan Basin, China. *Energies* **2022**, *15*, 8131. https://doi.org/10.3390/en15218131

Academic Editor: Mofazzal Hossain

Received: 26 May 2022
Accepted: 26 October 2022
Published: 31 October 2022

1. Introduction

A large fault damage zone generally comprises a narrow fault core and a wide damage zone that can be more than several kilometers [1,2]. The fracture network develops well along the fault damage zone and affects the fault zone's mechanical and petrophysical properties [1–4]. The fracture can greatly enhance the reservoir permeability and porosity and is of great importance in the deep (>4500 m) tight matrix reservoirs [5–9]. In the deep subsurface, seismic attributes (such as coherence, amplitude, variance, curvature, etc.) play an important role in describing the fault damage zone and its fractured reservoirs [10–16]. Recently, seismic process methods, such as maximum likelihood, structural tensor, and illumination have been used to image the deep fault damage zone and fractured reservoirs [8,9,17]. These methods could describe the envelope of the fault damage zone and the intensely fractured reservoirs in the deep subsurface. However, seismic characterization of the small fracture network is still a big challenge [8,9], which constrains the understanding of the "sweet spot" of the fractured reservoir and oil/gas exploitation in the deep subsurface.

The Permian-Triassic reef-shoal reservoir is a major exploration and development domain in the Sichuan Basin, SW China [18,19]. Large gas fields in Puguang, Longgang, and Yuanba areas have been discovered in reef-shoal reservoirs along the Kaijiang–Liangping platform margins [19–21]. Several studies described the reef-shoal microfacies

and reservoirs along the platform margins and proposed a microfacies-controlled reservoir model [18–23]. Some studies suggested that dolomitization had an important effect on the reef-shoal reservoir [24,25]. Further, dissolution porosity has become more important in the deep subsurface [21,23,26]. The seismic technologies of seismic amplitude attribute, bright spot, and prestack inversion have been used for reservoir description [21,27,28]. Although many techniques have been performed, there are still many low-production wells in the deep tight matrix reservoirs. On the other hand, a few wells that penetrated the fractured reservoirs could yield high gas production shown by the core investigation and production data [21,29]. This way, the "sweet spot" of the fractured reservoir could be a favorable target in the exploitation of the tight carbonate reservoir. In this area, several NE-trending thrust-fold belts have been found [21], but no strike-slip fault and related damage zone have been found yet. Considering little information on whether there is a large-scale fractured reservoir in the intracratonic basin, the seismic identification of the fault damage zone is a major issue in deep fractured reservoir exploitation.

For this purpose, we proposed a steerable pyramid method to identify the strike-slip fault and related damage zone in the Kaijiang–Liangping platform. With seismic-geological modeling and mapping of the fault damage zone, we suggested that the "sweet spot" of the fractured reservoir is a new favorable domain for gas development in the intracratonic Sichuan Basin.

2. Geological Background

The Sichuan Basin is an intracratonic basin in the northwestern Yangtze terrane, SW China (Figure 1a). This basin experienced a multi-stage tectonic-sedimentary cycle closely related to the opening-closing cycles from the Proto-Tethyan to Neo-Tethyan oceans [30–32]. In the process of multi-stage tectonic evolution, multiple unconformities developed among the Ediacaran-Cenozoic strata in the basin (Figure 1b). A series of fault-related structures formed in the periphery of the basin, and the central intracratonic basin presented a broad paleo-uplift [30].

The intracratonic Sichuan Basin has progressively deposited Ediacaran-Ordovician carbonates (Figure 1b). The central paleo-uplift formed in the Late Caledonian in the Late Ordovician-Silurian and subsequently absent in the Silurian-Carboniferous by the late Caledonian movement [30–32]. The Permian-Lower Triassic marine carbonates widely occur and are overlain by Mesozoic siliciclastic rocks through the Sichuan Basin. In the late Yanshanian movement during the Late Cretaceous and Himalayan movement from the Neogene, the intracratonic basin uplifted to form regional unconformities and strata gap (Figure 1). The Sichuan Basin has superior hydrocarbon accumulation conditions, with several sets of high-quality hydrocarbon source systems, such as the Upper Ediacaran-Lower Cambrian, Lower Silurian, Permian, Upper Triassic, and Lower Jurassic [33,34]. Carbonate gas reservoirs have been found in the Ediacaran, Cambrian, Carboniferous, and Permian-Triassic. In addition, the Silurian and Cambrian shale gas, Upper Triassic tight gas, and Jurassic tight oil/gas constitute multi-layer superimposed accumulations, which have become major gas exploration and development domains in China [35].

The Permian-Triassic reef-shoal facies are well developed along the Kaijiang–Liangping platform margins in the northern Sichuan Basin (Figure 1). Due to regional rifting occurring in the Middle Permian, a shallow SW-trending depression was gradually formed along a basement fault zone [22,23,36]. This intracratonic depression growth reached the peak at the deposited period of the Changxing Formation in the Late Permian and finally drowned gradually in the deposit period of the Feixianguan Formation in the Early Triassic [21–24]. The gentle carbonate ramps began to develop in the early period of the Changxing Formation and evolved into rimmed platform margins in the middle-late deposit period of the Changxing Formation (Figure 1c). The Changxing Formation is more than 300 m thick and comprises mudstone, bioclastic limestone, reef limestone, and thin dolomite. The sponge skeleton reef and sponge baffle reef occurred along the platform margins and were sporadic in the intraplatform [21,23]. Bioclastic shoals developed through the platform

margins and in the intraplatform. The Lower Triassic Feixianguan Formation consists of mudstone, oolitic limestone, and dolomite. Oolitic shoals developed in the early stage of the Feixianguan Formation and then gradually evolved into a restricted platform [22]. Both sides of the platform margins are favorable for the development of Permian-Triassic reef-shoal microfacies controlled by the carbonate reservoir distribution along the platform margins [36]. On the other hand, dolomitization, penecontemporaneous dissolution, and burial dissolution have enhanced the reef-shoal reservoirs with a large amount of secondary porosity [21–26]. In this way, the porosity and permeability of the reef-shoal reservoirs are variable in large ranges of 2–20% and 0.001–1000 mD, respectively [21–26]. Despite some high gas production wells, there are still many low-production wells in the deep tight matrix reservoirs. The Permian-Triassic reef-shoal bodies along the platform margins have been described by seismic technologies [21,27,28]. Due to the low resolution of the deep seismic data and the influence of Triassic evaporite, seismic velocity, and thrust-fold belt, there are generally ambiguous images of strike-slip faults from the seismic section.

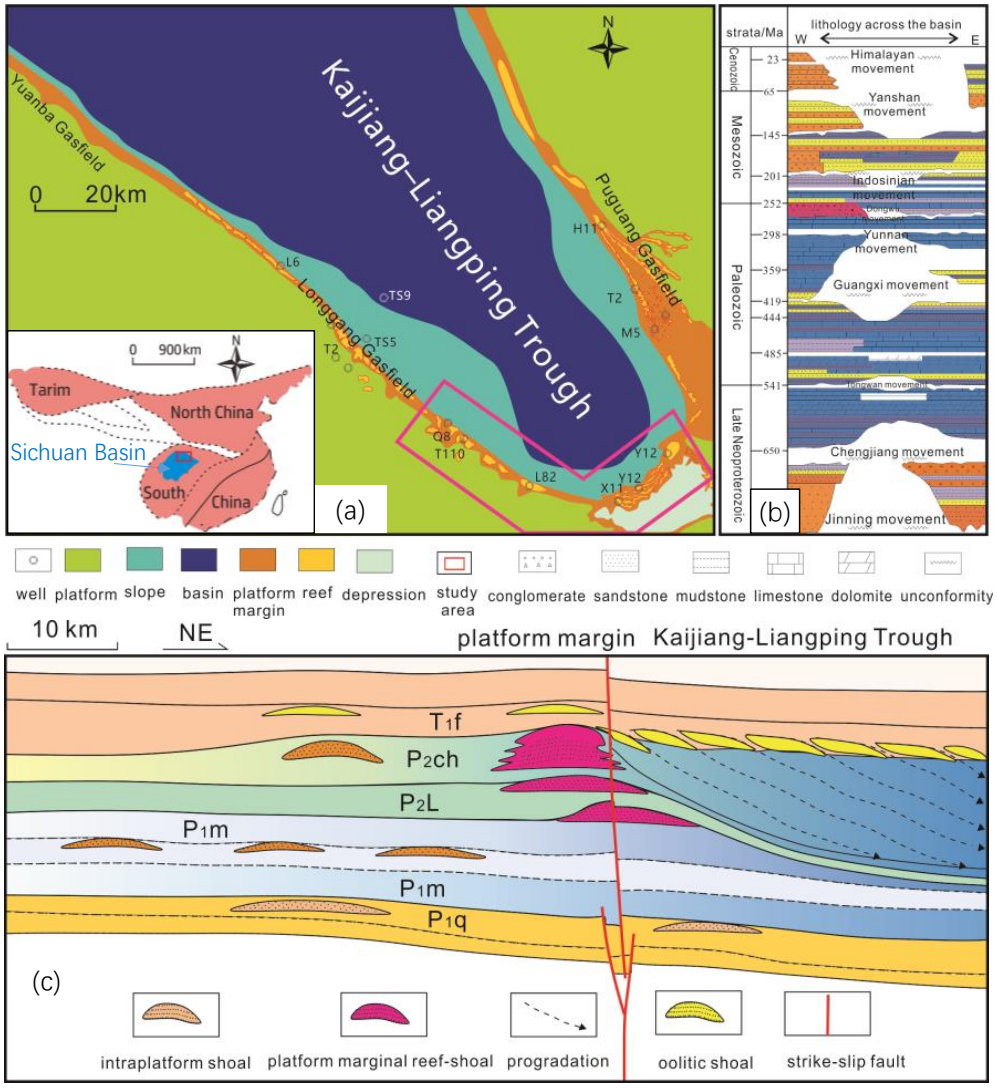

Figure 1. (**a**)The outline of the Kaijiang–Liangping Trough (Inset shows regional location), (**b**) the stratigraphic column, and (**c**) the geological section across the Permian-Triassic platform margin (revised from References [21,23,32]).

3. Data and Methods

More than 1000 km^2 of 3-D seismic surveys have been carried out in this study area. The seismic dataset used here has a bin spacing of 25 × 25 m with a main frequency of 30–40 Hz in the Permian carbonates, which are favorable for detailed fault mapping and seismic reservoir description. The main strata horizons are easily identified in seismic profiles and calibrated by more than ten wells. In the seismic resolution, vertical displacement of more than 10 m could be identified from the seismic sections. The structural complexity of fault damage zone and seismic resolution issues make identifying small faults and joints in deep fault damage zones difficult.

In this paper, we use the steerable pyramid [37,38] to extract an attribute that can reflect the damage zone of a strike-slip fault (Figure 2). The steerable pyramid includes two steps. The first step uses radial filters in the FK domain to steer seismic data into several bandpass-filtered components, which have different components corresponding to different scales. In the second step, planar filters with different directions are applied to each bandpass-filtered data. The amplitude absolute sum of the directional filtered data can be used to differentiate geological features [39]. For example, a directional filtered seismic horizon will have the largest absolute sum (name $|q|_{max}$) when the filter is parallel to the horizon and the smallest absolute sum (name $|q|_{min}$) when the filter is perpendicular to the horizon. For completeness, we denote $|q|_{mid}$ as the amplitude absolute sum of the filtered data with a filter direction perpendicular to the above two filters. It is easy to see that a seismic horizon follows the relationship $|q|_{max} \gg |q|_{mid} \approx |q|_{min}$. Using the notations given above, the attribute for the strike-slip fault damage zone is given as:

$$\frac{|q|_{mid} - |q|_{min}}{|q|_{max}}. \quad (1)$$

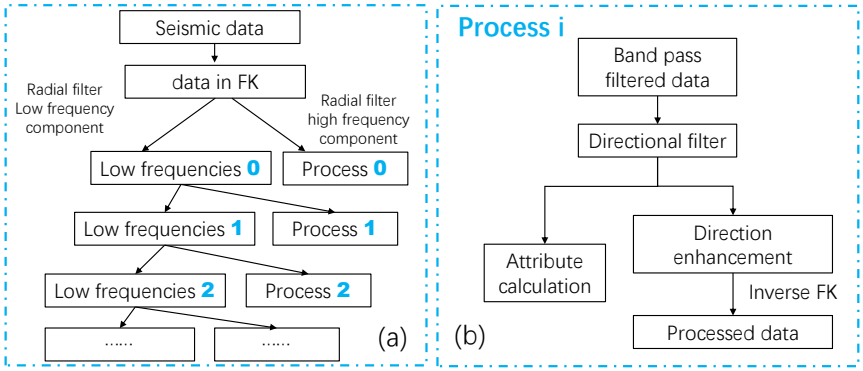

Figure 2. (**a**) Seismic process flowchart by the steerable pyramid method in this study area; (**b**) the flow diagram of a process in steerable pyramid processing.

This attribute is proposed by Mathewson and Hale (2008) to describe the local linear geological bodies such as channels [39]. In seismic data, the empirical experiments show that the attribute can also describe the strike-slip fault damage zone. The strike-slip fault breaks the planarity of the seismic horizon and thus increases the $|q|_{mid}$ as well as the attribute a little bit. More importantly, the attribute decreases to nearly zero when a data point moves from the strike-slip fault to the seismic horizon, making it a good indicator of the fault damage zone. In addition, it can be used to distinguish small-scale faults and joint assemblage, which is helpful for the description of internal structures in fault damage zones. On seismic profiles, the fault original strata layer is discontinuous with ambiguous wave impedance interface in the carbonate rocks. Generally, displacement across faults is small (<60 m), reflected on the seismic lines as not showing an obvious slip surface but rather a wide damage zone.

The workflow implemented in this research uses the steerable pyramid attribute with well data calibration. The fault damage zone boundary is constrained by the fracture elements shown in the well data. Generally, there is a breakup of the threshold value of the steerable pyramid attribute along the boundary of the fault damage zone. The stronger the fractured carbonate, the greater the intensity of the steerable pyramid amplitude attribute will be. In this way, the steerable pyramid amplitude attribute can be used to distinguish the fractured reservoirs along the fault damage zone from the surrounding rocks. In addition, steerable pyramid amplitude attributes in vertical strengthening along the strike-slip fault zone can suppress the influence of other geological factors (such as rivers, reef-shoal facies, etc., which have a shorter longitudinal extension than the fault damage zone), which helps the description of the fault damage zone. The seismic processing flowchart is as Figure 2.

4. Characteristics of the Strike-Slip Fault and Related Fault Damage Zones

4.1. The Strike-Slip Fault Zone

By the steerable pyramid processing, the seismic resolution has been enhanced for strike-slip fault identification. The seismic noises could be suppressed to show a clear vertical fault zone in the deep strata. Some strike-slip faults present clearer fault planes than the continuous flexural reflection or ambiguous fault reflection in the seismic sections (Figure 3). Some small faults could also be identified by vertical deflection or offset images. In the processed seismic planar attributes, the strike-slip fault could be imagined by a more distinct fault trace. In addition, some vertical chaotic reflections indicate the strike-slip fault zones. In this way, the seismic steerable pyramid processing enhanced the fault image accuracy.

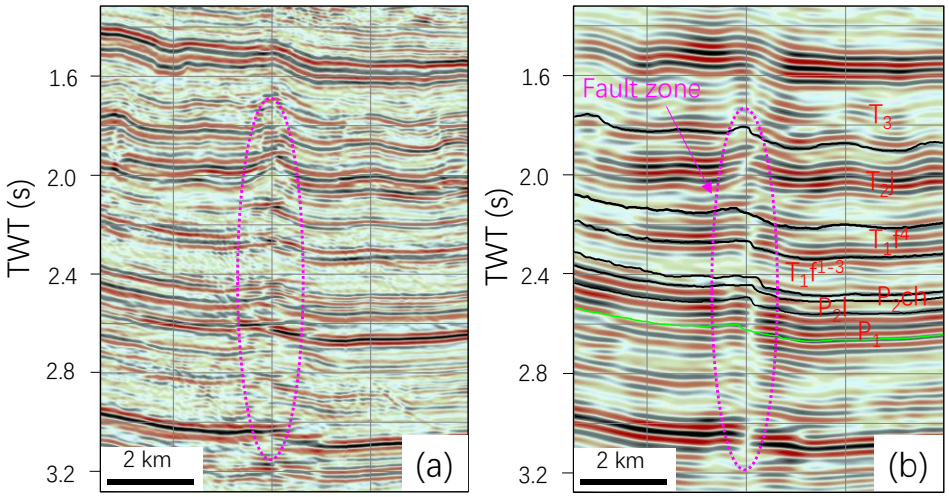

Figure 3. (**a**) A seismic section and (**b**) its processed section by steerable pyramid processing in this study area (the red arrows indicate strike-slip fault).

Based on strike-slip fault identification and typical strike-slip fault structural modeling, seismic coherence and amplitude attributes were selected to identify strike-slip faults. The seismic profile shows that strike-slip faults are mainly distributed from the basement to the Triassic (Figures 4 and 5). The strike-slip faults have distinct longitudinal stratification characteristics with three structural layers Ordovician-basement, Silurian-Carboniferous, and Permian-Triassic. In different layers, there are different structural styles and fault distributions. The lower structural layer is dominated by transtensional faults, and a series of strike-slip faults end up in the Ordovician, revealing the early strike-slip fault activities. Most of these strike-slip faults developed upward to the bottom of the Permian system, and presented the characteristics of transpressional faults, which are different from the transtensional faults in the lower part. At the same time, it spreads vertically upward to form a wider flower structure in the Permian-Triassic and converges downward into the

deep main fault. These faults show significant inherited development characteristics, but there are some differences in profile characteristics and plane combination, representing different periods of fault activity. A small number of faults extend up to the Triassic system and spread upward, mainly linear echelon faults, and develop negative flower structure, weak fault activity for an inherited development.

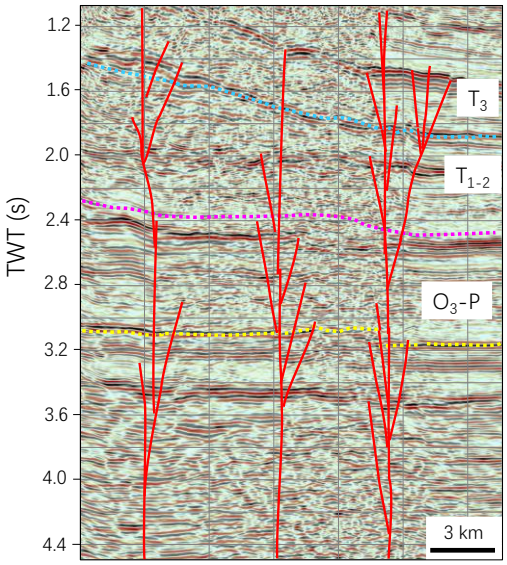

Figure 4. Typical seismic section showing three layered fault zones in this study area (T_3: the Upper Triassic; $T_{1–2}$: the Lower-Middle Triassic; P: the Permian; O_3: the Upper Ordovician).

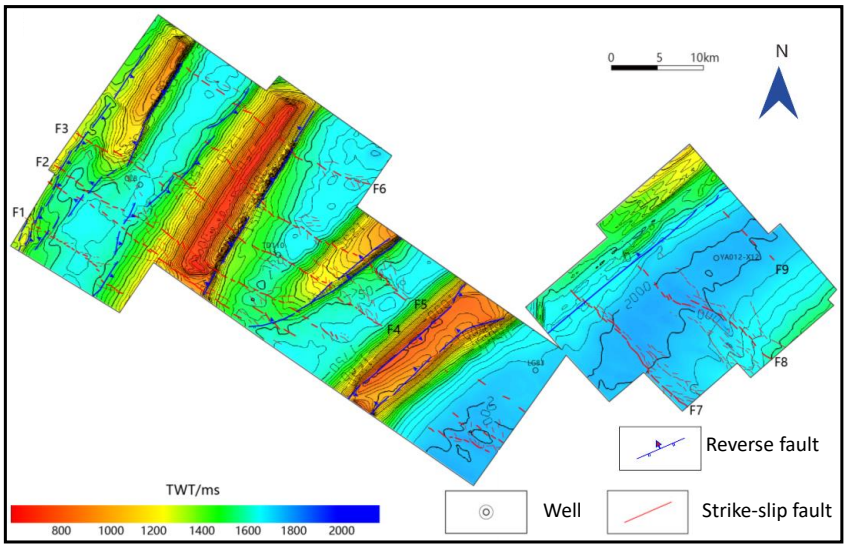

Figure 5. The strike-slip fault distribution in the Triassic of this study area.

By structural modeling and strike-slip fault identification, a 3D seismic interpretation of the strike-slip fault has been carried out in this study area. We found a series of NW-trending strike-slip faults developed in the study area (Figure 5). Six NW-trending strike-slip fault zones developed in the western 3D area and three fault zones in the extended eastern more than 50 km. Three NW-trending strike-slip faults have been identified in the northeastern area, which may extend to the interior of the trough in the northwest direction. These strike-slip faults are distributed intermittently, with a total length of 290 km. In the plane, the linear structure mainly composes of the combination of en echelon or oblique faults, and the strike-slip fault zone has a low through-going, indicating a low maturity

of strike-slip faults. In a few hard-linked segments, R shear faults occurred along the major faults, horsetail structure may occur at the fault tips, and a few minimal horst and graben may occur at localized overlapping zones. The secondary fault generally displays a linear fault plane with unclear vertical displacement. In this way, the major fault zone can be mapped by the seismic attributes and fault modeling, but it is difficult to identify the secondary faults and their assemblages.

4.2. Fault Damage Zone

Although the joints cannot be identified from the seismic profile, the steerable pyramid attribute improved the image of the damage zone by scanning the whole seismic data volume and calculating the similarity between data samples. In this study, we manually analyzed the seismic reflection characteristics of fault damage zones and carried out damage zone strengthening under dip-angle control. In order to characterize the fault damage zone, a discontinuous attribute body is used to describe the plane and longitudinal distribution characteristics of the damage zone. In this way, the discontinuous attribute processed by the steerable pyramid can clearly reflect the vertical and planar distribution characteristics of the fault damage zone (Figure 6). The integration of this attribute volume with conventional 3D seismic data can analyze the longitudinal growth and connectivity of the fault damage zone.

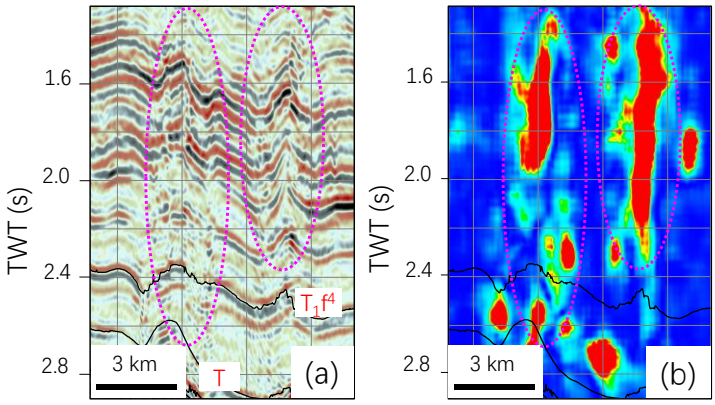

Figure 6. (**a**) The original seismic profile (T_1f^4: the fourth member of Feixianguan Formation of the Lower Triassic; T: base of the Triassic), and (**b**) the steerable pyramid attribute profile in the western Kaijiang-Liangping Trough (the red-green color area shows the fault damage zone, and the blue area shows the host rock).

In the study area, the fault damage zone is almost vertical along the strike-slip fault (Figure 6b). The bright color stripes in Figure 6b may present the intensity of the fault damage zone. The large fault zone generally showed a wide fault damage zone and stronger deformation intensity. Generally, there are symmetrical damage zones along the major fault plane. It is noted that the response of the fault damage zone varies vertically and presents discontinuous seismic waves, which suggests that the fault damage zone width and intensity changed rapidly in vertical view and has not connected to a through-going damage zone. By well calibration, we see that the wide damage zone with strong intensity is generally developed in the Permian-Triassic carbonate rocks. The damage zone is consistent with the contemporaneous fault activity and feasible damage of the carbonate rocks. In addition, the unconnected damage zone suggests an immature fault zone and some oblique fracture assemblages in the vertical view. Their unclear vertical displacement showed weak deformation.

In plane view, the fault damage zones are distributed along the fault strike (Figure 7). The fault damage zone width generally varied between 50 and 300 m. The wide fault damage zone suggests strong interaction and deformation in the overlapping area. The fault overlap zone with a wider fault zone shows varied deformation and fault combinations. The

relatively small segments are almost linearly extended with the smaller width. Generally, the deformation intensity of the fault damage zone varied along the fault strike, consistent with the vertical attribute, which suggests that the fault zone has segmentation with isolated fault segments or the unconnected fault zone.

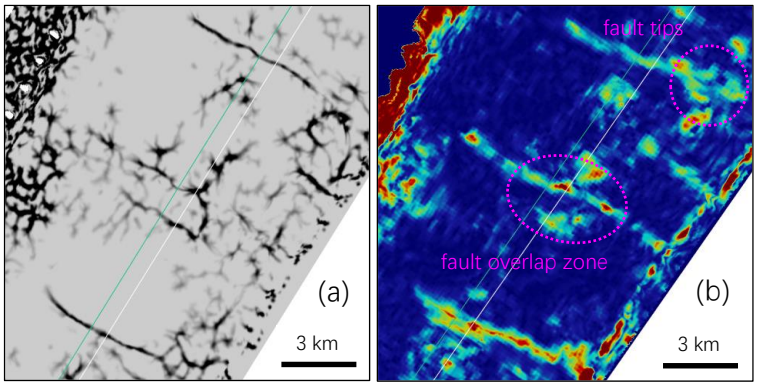

Figure 7. (**a**) Seismic coherence plane attribute and (**b**) processed by steerable pyramid in the study area.

By the correction of the combination of the fault damage zone network in the seismic profile and plane attribute, a 3D visualization map can be formed to show the fault damage zone (Figure 8). The results show that the steerable pyramid attribute can be used to describe the spatial network along the fault damage zone. The fracture length, width, and intensity can be 3D visualized. In the steerable pyramid attribute, there are clear internal structures and distinct segmentation along the NW-trending fault zone. The major fault comprises multiple damage zones in overlapping and oblique combinations. The steerable pyramid attribute shows a better effect than other attributes. Steerable pyramid attributes can describe small faults and the internal structure in the fault zone and have a certain effect on the joint prediction that cannot be obtained by coherent attribute.

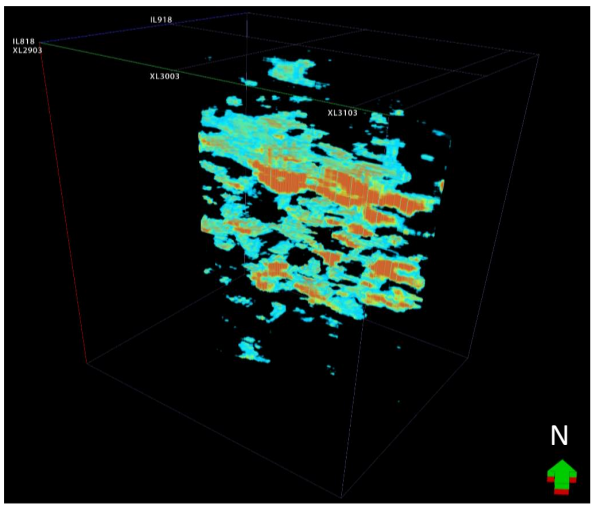

Figure 8. Three dimensional visualization of a strike-slip fault damage zone by the steerable pyramid attribute in the study area.

5. Discussions

5.1. Seismic Description of Fault Damage Zone

In deep tight reservoirs, seismic technology has been widely used in the fracture network description [10–17]. Constrained by low-resolution seismic data, the conventional

seismic methods are generally unfavorable in the identification of deep fractured reservoirs along the fault damage zones.

In the deep subsurface, the fractured structures along the carbonate strike-slip fault zone are generally the main targets for productive wells in the Tarim Basin [40,41]. Owing to the challenge in identifying the fractures from the deep subsurface, the fault damage zone prediction and description of this fault damage zone are significant for the oil/gas high production wells in the deep tight carbonate reservoirs. Methods of AFE (Automatic fault extraction), ant body, and structure tensor were used to describe the carbonate fault damage zone [8,17]. In this study area, the strike-slip faults with small vertical displacement (<20 m) are more difficult to identify than the conventional seismic sections. Compared with other methods, the steerable pyramid processed attribute is sensitive to the fault damage zone and can better image the boundary of the damage zones. Even without the well data calibration, the steerable pyramid processed attribute can present clear boundaries of the fractured reservoir in the damage zone. Through the correlation analysis, there is a positive correlation between the logging permeability and steerable pyramid processed attribute value for the fractured reservoirs. In this way, 3D fractured reservoirs can be obtained from the 3D steerable pyramid processed attribute body (Figure 7). Integrated with the 3D fractured reservoirs, the relationship between the fractures and reservoirs can be shown in 3D visualization. For these reasons, the steerable pyramid attribute is helpful for well trajectory design and drilling monitoring along the fault damage zone in this kind of reservoir.

In this study area, there are ambiguous seismic responses for the small faults and damage zone below the thrust-fold belts and thick evaporites. The steerable pyramid attribute and other seismic attributes are unfavorable in these areas. In addition, many fault zones in the broad areas showed distinct damage boundaries from the steerable pyramid attribute (Figures 6–8). However, there are still some fault damage zones that present unclear damage boundaries. This is possibly related to the small fault damage zone without internal boundaries in the deep subsurface and/or low seismic resolution in this area. Due to a few wells penetrating into the fault damage zones, the exact boundaries of the fault damage zones still need to be confirmed by more wells. Further, a few abnormal steerable pyramid attributes can be attributed to the microfacies and lithological variation along the fault damage zones. It noted that the highlighted intense steerable pyramid attributes are used to indicate the permeable fracture zones or fractured reservoirs. This could be consistent with the "sweet spot" fracture-cave reservoirs in the Tarim Basin. However, it needs further drilling to reveal whether they are a "sweet spot" or just filled fracture zones.

5.2. The Distribution of the Fault Damage Zone and Effect on Carbonate Reservoir

By seismic identification, the carbonate fault damage zones are distributed as band shapes and fan-shapes along the fault zone. The width and intensity are variable along the fault strike and in the vertical section (Figures 6–8). This is consistent with the immature en echelon/oblique faults with low displacement (Figure 5). The width of the fault damage zones is generally in the range of 100–500 m and could be up to 2000 m in the carbonate rocks. The results indicate that the higher vertical displacement can be measured in the seismic section and presents wider damage zone width. This is consistent with a power-law correlation between the width of the fault damage zone and the fault displacement [2,14], although the horizontal displacement is hard to be measured by the low-resolution seismic data. This suggests that the growth of the fault damage zone is closely related to fault propagation, particularly during the immature period of isolated en echelon/oblique faults. Further, the fault intersection area, fault overlap zone, and scattered fault tips generally show wide fault damage zones (Figure 7). With the progressive fault linkage and interaction, the overlapping and intersection areas are becoming the major deformation and fractured zones. In this way, a more than 1000 m wide fault damage zone could occur along the fault zone.

With the cores and logging data analysis, the fracture network and fractured reservoir mainly occurred along the fault damage zones and the axis of the fault-related fold. In the Permian carbonate, the larger the fault scale generally led to the wider the fault damage zone width. All of the much higher gas production wells have penetrated the fracture network, in which almost all the wells have fallen into the fault damage zones. The fractures are characterized by high dip angles along the fault damage zones, and three stages of fracture activities with carbonate cements, asphaltene filling and un-filled fractures in the Yuanba Gasfield [28]. Particularly, the dissolution pores developed well along the fractures. In this way, the permeability could be increased more than 1–2 orders of magnitude, and the porosity could be enhanced more than one time than the matrix reservoirs. In addition, hydrocarbon dissolution and later burial dissolution are of great importance in reservoir improvement, which could be closely related along the fracture network in the fault damage zone.

In this case, the carbonate reservoirs are at a depth of more than 5000 m. Most primary porosity has been lost by cementation during burial, with a matrix porosity of the reservoir being less than 10% and permeability generally less than 2 mD. In this way, the fracture developed damage zone plays an important role in gas production. Based on strike-slip fault interpretation, we carried out a variety of seismic attributes and well control inversion for fractured reservoir identification. The well data indicate that the fault damage zone and fractured reservoirs are consistent with the stronger steerable pyramid attribute. Owing to the varied fracture network along the fault damage zone, the fractured reservoir shows varied steerable pyramid attribute values along the fault damage zone (Figure 8). The fractured reservoir boundary from the steerable pyramid attribute is notable in the seismic profile. The relative location is consistent with drilling results from well data. For example, the well gas production is generally lower than 200,000 m^3/d in the study area. However, well T110 had much higher gas production up to 580, 000 m^3/d. Although T110 has not penetrated a fault zone in other data (Figure 9a), it showed that the well was just through the fault damage zone in the steerable pyramid processed profile (Figure 9b). On the other hand, well Q8 is generally thought to have penetrated the intense fault damage zone in the conventional seismic profile (Figure 9a). However, the gas production is much lower at 158,000 m^3/d. In our processed profile (Figure 9b), the well just crosses the weak damage zone of the Permian carbonates.

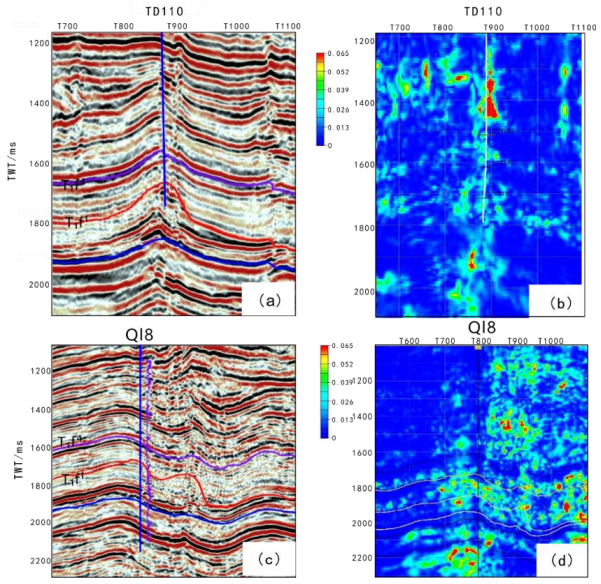

Figure 9. Seismic profiles (**a**,**c**) and steerable pyramid processed attribute profiles (**b**,**d**) of well TD110 and Ql8, respectively. The green-red blocks show the fractured reservoirs along the fault damage zone. (T_1f^4: fourth member of the Feixianguan Formation in the Lower Triassic; T_1f: base Feixianguan Formation of the Lower Triassic; P_2ch: Changxing Formation of the Permian).

6. Conclusions

The implementation of the steerable pyramid method in the Sichuan Basin has shown that:

(1) Steerable pyramid processing enhanced the seismic imaging of the small strike-slip faults and found a series of NW-trending strike-slip faults in the Kaijiang–Liangping area.
(2) The steerable pyramid attribute revealed distinct vertical and horizontal boundaries of the fault damage zone, and the un-through-going fault damage zone in the deep subsurface. The steerable pyramid method is favorable for the identification of fault damage zone along the weak strike-slip fault zones.
(3) The width of the fault damage zone generally varied in the range of 100–500 m which is closely related to fault displacement, and the fault overlapping and interaction could result in a much wider damage zone.
(4) The fault damage zone could play a constructive role in high gas production in the deep tight carbonate reservoir and is a new favorable exploitation domain in the Sichuan Basin.

Author Contributions: Conceptualization, Q.T. and B.L.; methodology, S.T. and G.W.; software, S.T. and S.L.; investigation, B.L., X.L. and L.F.; data curation, B.L., X.L. and L.F.; writing—original draft preparation, G.W. and S.T.; visualization, S.T. and S.L.; supervision, Q.T. and B.L.; funding acquisition, Q.T. and B.L. All authors have read and agreed to the published version of the manuscript.

Funding: Science and Technology Cooperation Project of the CNPC-SWPU Innovation Alliance (2020CX010101 and 2020CX010301) and the National Natural Science Foundation of China (41972121).

Acknowledgments: The authors thank the editors and reviewers for their comments regarding manuscript improvement. We also thank Xihui Xu, Xiaojun Zhou, Weizhen Tian, Bingshan Ma and Yonghong Wu for their help in data and visualization.

Conflicts of Interest: The authors declare no conflict of interest.

References

1. Torabi, A.; Berg, S.S. Scaling of fault attributes: A review. *Mar. Pet. Geol.* **2011**, *28*, 1444–1460. [CrossRef]
2. Choi, J.H.; Edwards, P.; Ko, K.; Kim, Y.S. Definition and classification of fault damage zones: A review and a new methodological approach. *Earth Sci. Rev.* **2016**, *152*, 70–87. [CrossRef]
3. Faulkner, D.R.; Jackson, C.A.L.; Lunn, R.J.; Schlische, R.W.; Shipton, Z.K.; Wibberley, C.A.J.; Withjack, M.O. A review of recent developments concerning the structure, mechanics and fluid flow properties of fault zones. *J. Struct. Geol.* **2010**, *32*, 1557–1575. [CrossRef]
4. Bense, V.F.; Gleeson, T.; Loveless, S.E.; Bour, O.; Scibek, J. Fault zone hydrogeology. *Earth Sci. Rev.* **2013**, *127*, 171–192. [CrossRef]
5. Spencer, C.W. Review of characteristics of low-permeability gas reservoirs in Western United States. *AAPG Bull.* **1989**, *73*, 613–629.
6. Garland, J.; Neilson, J.; Laubach, S.E.; Whidden, K.J. Advances in carbonate exploration and reservoir analysis. *Geol. Soc. Lond. Spec. Publ.* **2012**, *370*, 1–15. [CrossRef]
7. Sun, L.D.; Zou, C.N.; Zhu, R.K.; Zhang, Y.H.; Zhang, S.C.; Zhang, B.M.; Zhu, G.Y.; Gao, Z.Y. Formation, distribution and potential of deep hydrocarbon resources in China. *Pet. Explor. Dev.* **2013**, *40*, 687–695. [CrossRef]
8. Wang, Q.H.; Zhang, Y.T.; Xie, Z.; Zhao, Y.W.; Zhang, C.; Sun, C.; Wu, G.H. The advancement and challenges of seismic technique on the ultra-deep carbonate reservoir exploitation in the Tarim Basin, western China. *Energies* **2022**, *15*, 7653. [CrossRef]
9. He, X.; Guo, G.A.; Tang, Q.S.; Wu, G.H.; Xu, W.; Ma, B.S.; Huang, T.J.; Tian, W.Z. The advance and challenge of the Ediacaran fractured reservoir development in the central Sichuan Basin, China. *Energies* **2022**, *15*, 8137. [CrossRef]
10. Iacopini, D.; Butler, R.W.H.; Purves, S.; McArdle, N.; De Freslon, N. Exploring the seismic expression of fault zones in 3D seismic volumes. *J. Struct. Geol.* **2016**, *89*, 54–73. [CrossRef]
11. Botter, C.; Cardozo, N.; Hardy, S.; Lecomte, I.; Paton, G.; Escalona, A. Seismic characterization of fault damage in 3D using mechanical and seismic modeling. *Mar. Pet. Geol.* **2016**, *77*, 973–990. [CrossRef]
12. Torabi, A.; Alaei, B.; Kolyukhin, D. Analysis of fault scaling relations using fault seismic attributes. *Geophys. Prospect.* **2017**, *65*, 581–595. [CrossRef]
13. Liao, Z.H.; Carpenter, B.M.; Marfurt, K.J.; Reches, Z.E. Analysis of fault damage zones using three-dimensional seismic coherence in the Anadarko Basin, Oklahoma. *AAPG Bull.* **2019**, *103*, 1771–1785. [CrossRef]
14. Ma, D.B.; Wu, G.H.; Scarselli, N.; Luo, X.S.; Han, J.F.; Chen, Z.Y. Seismic damage zone and width–throw scaling along the strike-slip faults in the Ordovician carbonates in the Tarim Basin. *Pet. Sci.* **2019**, *16*, 752–757. [CrossRef]

15. Ahmad, N.; Khan, S.; Noor, E.F.; Zou, Z.; Al-Shuhail, A. Seismic data interpretation and identification of hydrocarbon-bearing zones of Rajian area, Pakistan. *Minerals* **2021**, *11*, 891. [CrossRef]
16. Zhao, Z.; Liu, J.; Ding, W.; Yang, R.; Zhao, G. Analysis of seismic damage zones: A case study of the Ordovician formation in the Shunbei 5 fault zone, Tarim Basin, China. *J. Mar. Sci. Eng.* **2021**, *9*, 630. [CrossRef]
17. Wang, R.; Yang, J.; Chang, L.; Zhang, Y.; Sun, C.; Wan, X.; Wu, G.; Bai, B. 3D modeling of fracture-cave reservoir from a strike-slip fault-controlled carbonate oilfield in Northwestern China. *Energies* **2022**, *15*, 6415. [CrossRef]
18. Wen, L.; Zhang, Q.; Yang, Y.; Liu, H.Y.; Che, Q. Factors controlling reef-bank reservoirs in the Changxing-Feixianguan formation in the Sichuan Basin and their play fairways. *Nat. Gas Ind.* **2012**, *32*, 39–44, (In Chinese with English abstract).
19. Dong, Q.M.; Hu, Z.G.; Chen, S.Y.; Yuan, B.G.; Dai, X. Reef–shoal combinations and reservoir characteristics of the Changxing–Feixianguan Formation in the eastern Kaijiang–Liangping trough, Sichuan Basin, China. *Carbon. Evapor.* **2021**, *36*, 24. [CrossRef]
20. Ma, Y.S.; Guo, X.S.; Guo, T.L.; Huan, R.; Cai, X.Y.; Li, G.X. The Puguang gas field: New giant discovery in the mature Sichuan Basin, southwest China. *AAPG Bull.* **2007**, *91*, 627–643. [CrossRef]
21. Guo, X.; Hu, D.; Li, Y.; Duan, J.; Ji, C.; Duan, H. Discovery and theoretical and technical innovations of Yuanba gas field in Sichuan Basin, SW China. *Pet. Explor. Dev.* **2018**, *45*, 14–26. [CrossRef]
22. Chen, L.; Lu, Y.C.; Fu, X.Y.; Xing, F.C.; Wang, C.; Luo, C. Oolitic shoal complexes characterization of the Lower Triassic Feixianguan Formation in the Yuanba Gas Field, Northeast Sichuan Basin, China. *Mar. Pet. Geol.* **2017**, *83*, 35–49. [CrossRef]
23. Long, S.X.; You, Y.C.; Jiang, S.; Liu, G.P.; Feng, Q.; Gao, Y.; Niu, X.F. Integrated characterization of ultradeep reef-shoal reservoir architecture: A case study of the Upper Permian Changxing Formation in the giant Yuanba gas field, Sichuan Basin, China. *J. Pet. Sci. Eng.* **2020**, *195*, 107842. [CrossRef]
24. Jiang, L.; Worden, R.H.; Cai, C.F.; Li, K.K.; Xiang, L.; Cai, L.L.; He, X.Y. Dolomitization of gas reservoirs: The Upper Permian Changxing and Lower Triassic Feixianguan Formations, Northeast Sichuan Basin, China. *J. Sediment. Res.* **2014**, *84*, 792–815. [CrossRef]
25. Zhou, J.G.; Deng, H.Y.; Yu, Z.; Guo, Q.; Zhang, R.; Zhang, J.Y.; Li, W.Z. The genesis and prediction of dolomite reservoir in reef-shoal of Changxing Formation-Feixianguan Formation in Sichuan Basin. *J. Pet. Sci. Eng.* **2019**, *178*, 324–335. [CrossRef]
26. Huo, F.; Wang, X.Z.; Wen, H.G.; Xu, W.L.; Huang, H.W.; Jiang, H.C.; Li, Y.W.; Li, B. Genetic mechanism and pore evolution in high quality dolomite reservoirs of the Changxing-Feixianguan Formation in the northeastern Sichuan Basin, China. *J. Pet. Sci. Engin.* **2020**, *194*, 107511. [CrossRef]
27. Gong, X.X.; Yang, W.; Li, W.J.; Zhou, X.G.; Tang, Q.S.; Zhang, J. Characteristics and geological properties of seismic bright spots in the Permian carbonate deposit, Changhsing Formation, Longgang Area, Northeast Sichuan Basin, China. *Carbon. Evapor.* **2020**, *35*, 98. [CrossRef]
28. Zhou, L.; Zhong, F.Y.; Yan, J.C.; Zhong, K.X.; Wu, Y.; Xu, X.H.; Lu, P.; Zhang, W.J.; Liu, Y. Prestack inversion identification of organic reef gas reservoirs of Permian Changxing Formation in Damaoping area, Sichuan Basin, SW China. *Pet. Explor. Dev.* **2020**, *47*, 89–100. [CrossRef]
29. Fan, X.J.; Peng, J.; Li, J.X.; Chen, D.; Li, F.; Deng, J.H.; Huang, Y.; Miao, Z.W. Fracture characteristics of ultra-deep reef-bank lithologic gas reservoirs in the Upper Permian Changxing Formation in Yuanba area, northeastern Sichuan Basin. *Oil Gas Geol.* **2014**, *35*, 511–516.
30. He, D.F.; Li, D.S.; Zhang, G.W.; Zhao, L.Z.; Fan, C.; Lu, R.Q.; Wen, Z. Formation and evolution of multi-cycle superposed Sichuan Basin, China. *Chin. J. Geol.* **2011**, *46*, 589–606.
31. Li, H.K.; Li, Z.Q.; Long, W.; Wan, S.S.; Ding, X.; Wang, S.Z.; Wang, Z.Z. Vertical configuration of Sichuan Basin and its superimposed characteristics of the prototype basin. *J. Chengdu Univ. Technol.* **2019**, *46*, 257–267, (In Chinese with English abstract).
32. Gu, Z.D.; Wang, Z.C.; Hu, S.Y.; Wang, H.; Yin, J.F.; Huang, P.H. Tectonic settings of global marine carbonate giant fields and exploration. *Nat. Gas Geosci.* **2012**, *23*, 106–118.
33. Zou, H.Y.; Hao, F.; Zhu, Y.M.; Guo, T.L.; Cai, X.Y.; Li, P.P.; Zhang, X.F. Source rocks for the giant Puguang Gas Field, Sichuan Basin: Implication for petroleum exploration in marine sequences in South China. *Acta Geol. Sin.* **2008**, *82*, 477–486.
34. Hu, G.Y.; He, F.; Mi, J.K.; Yuan, Y.L.; Guo, J.H. The geochemical characteristics, distribution patterns, and gas exploration potential of marine source rocks in northwest Sichuan Basin. *Nat. Gas Geosci.* **2021**, *32*, 319–333.
35. Zou, C.N.; Du, J.H.; Xu, C.C.; Wang, Z.C.; Zhang, B.M.; Wei, G.Q.; Wang, T.S.; Yao, G.S.; Deng, S.W.; Liu, J.J.; et al. Formation, distribution, resource potential and discovery of the Sinian-Cambrian giant gas field, Sichuan Basin, SW China. *Pet. Explor. Dev.* **2014**, *41*, 278–293. [CrossRef]
36. Wang, X.Z.; Li, B.; Wen, L.; Xu, L.; Xie, S.Y.; Du, Y.; Feng, M.Y.; Yang, X.F.; Wang, Y.P.; Pei, S.Q. Characteristics of "Guangyuan-Wangcang" trough during late Middle Permian and its petroleum geological significance in northern Sichuan Basin, SW China. *Pet. Explor. Dev.* **2021**, *48*, 562–574. [CrossRef]
37. Freeman, W.T.; Adelson, E.H. The design and use of steerable filters. *IEEE Trans. Pattern Anal. Mach. Intell.* **1991**, *13*, 891–906. [CrossRef]
38. Luche, C.; Denis, F.; Baskurt, A. 3d steerable pyramid based on conic filters. *Proc. SPIE* **2004**, *5266*, 260–268.
39. Mathewson, J.M.; Hale, D. Detection of channels in seismic images using the steerable pyramid. *Seg. Tech. Program Expand. Abstr.* **2008**, 859–863.

40. Yang, X.W.; Wang, R.J.; Deng, X.L.; Li, S.Y.; Zhang, H.; Yao, C. Theoretical exploration and practice of water injection gravity flooding oil in ultra-deep fault-controlled fractured-cavity carbonate reservoirs. *Pet. Explor. Dev.* **2022**, *49*, 133–143. [CrossRef]
41. Wu, G.H.; Zhao, K.Z.; Qu, H.Z.; Nicola, S.; Zhang, Y.T.; Han, J.F.; Xu, Y.F. Permeability distribution and scaling in multi-stages carbonate damage zones: Insight from strike-slip fault zones in the Tarim Basin, NW China. *Mar. Pet. Geol.* **2020**, *114*, 104208. [CrossRef]